Environ. Sci. Technol. **1999**, *33,* 2418−2424

Atrazine Degradation in Irradiated Iron/Oxalate Systems: Effects of pH and Oxalate

MARIANNE E. BALMER AND BARBARA SULZBERGER*

Swiss Federal Institute of Environmental Science and Technology (EAWAG), CH-8600 Dübendorf, Switzerland

The purpose of this study was to examine the various factors that control the kinetics of atrazine degradation in irradiated Fe(III)/oxalate systems, in the following denoted as photo-Fenton systems. In these systems, attack by hydroxyl radicals (HO•) was the only pathway of atrazine degradation. Transformation of pollutants by HO• that are produced in photo-Fenton systems is of interest in atmospheric waters, in iron-rich surface waters, and possibly on soil surfaces. Studies were conducted in systems containing 6 μM iron and 0, 18, and 180 μM oxalate at $3 \leq$ pH ≤ 8, irradiated with simulated sunlight. Both oxalate concentration and pH greatly affected the rate of atrazine transformation. In the presence of initial 18 μM oxalate, the rate increased in the order of pH 7.5 < 5.6 < 3.2 < 4.3, and with 180 μM in the order of pH 7.9 < 3.2 < 4.6 ≈ 5.4. At all pH values, the rates were considerably higher at the higher initial oxalate concentration. In both cases, no degradation occurred at pH > 7. In the absence of oxalate, atrazine transformation was slower and occurred only up to pH 4.1. These experimental results can be explained by various competing effects. First, both pH and oxalate concentration control the iron(III) speciation and thus the rate of photolysis of Fe(III) complexes. Second, also the Fe(II) speciation and hence the rate of the Fenton reaction [oxidation of Fe(II) by H_2O_2] are affected by pH and oxalate concentration. Finally, oxalate acts as a scavenger of hydroxyl radicals that are produced in the Fenton reaction and hence competes with atrazine for HO•. We have identified the individual reactions taking place in these complex systems at pH 3 by combining batch experiments with kinetic modeling.

Introduction

The hydroxyl radical (HO•) is the most reactive oxidant known in the environment, with second-order rate constants for most organic compounds of 10^8−10^{10} M^{-1} s^{-1} (e.g., see refs *1*−*3*). In various environmental compartments, the oxidation of photochemically produced Fe(II) by H_2O_2 (reaction sequence in photo-Fenton systems, see below) is an important source of HO• (*4*−*6*). We define photolysis of iron(III) complexes and subsequent Fenton reaction as photo-Fenton systems (Figure 1). Since iron is one of the most abundant elements in fogwater, rainwater, and aerosol particles (*7*), the reaction sequence in photo-Fenton systems is an important pathway of HO• production in atmospheric waters. In most surface waters, the major sources of HO• are photochemical reactions of the water constituents NO_3^- and colored dissolved organic matter (*8*, *9*). In iron-rich surface waters, the reaction sequence in photo-Fenton systems may be a significant additional source of HO•. In iron-rich environmental compartments with low DOC content, photolysis of Fe(III)−hydroxo complexes also contributes to HO• production (*10*, *11*). Many soils have a high content of iron oxides and iron hydroxides, of humic acids, and of simple carboxylic acids such as oxalate (*12*). Hence, one can expect that Fe(III) complexes on soil surfaces undergo photochemical reactions. In model systems with Fe(III)-hydroxide suspensions, photo-Fenton systems have been shown to be an important source of HO• (*6*).

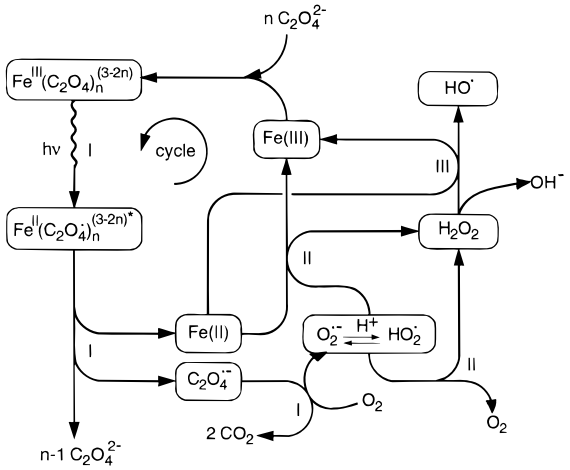

FIGURE 1. Iron cycling and main reactions in oxalate-containing photo-Fenton systems. Adapted from ref *29*.

This study investigates the pH dependence and the effect of different concentrations of an organic complexing agent on the kinetics of transformation of a probe pollutant by HO• attack in photo-Fenton systems. Irradiated model systems were therefore studied, in which oxalate served as reducing agent, and atrazine as probe pollutant. In contrast to earlier studies published in the literature, which were carried out only at low pH, we investigated the systems over the entire environmentally relevant pH range: $3 \leq$ pH ≤ 8. Furthermore, we identified the important reactions and equilibria in these complex photo-Fenton systems by combining batch experiments with kinetic modeling.

We have chosen atrazine as a probe compound because this synthetic organic chemical is still one of the most widely used herbicides worldwide. It shows a relatively high persistence in soils (half-life of weeks to months) (*13*, *14*), and in aquatic systems, atrazine is known to behave nearly conservatively except for the proposed degradation by photochemically produced OH radicals (*15*, *16*). The mechanisms and product formation of reaction of atrazine with HO• have been studied carefully in experimental systems where OH radicals were formed through different pathways: (i) by photolysis of nitrate (*17*), (ii) in the Fenton reaction (*18*), and (iii) upon irradiation of TiO_2 colloidal particles, where the photoholes react with surface hydroxide groups to produce HO• (*19*). Hitherto, atrazine degradation in photo-Fenton systems has not been investigated in a systematic way.

Photo-Fenton System. Figure 1 shows the various reactions and the intermediates and products formed in a photo-Fenton system with Fe(III)−oxalate complexes being photolyzed. Thereby, Fe(II) and the superoxide/hydroperoxyl radicals ($O_2^{\bullet-}$/HO•) are key intermediates. These intermediates are formed via the following processes (reactions I in Figure 1): (i) ligand-to-metal charge-transfer transition

10.1021/es9808705 CCC: $18.00
Published on Web 06/05/1999

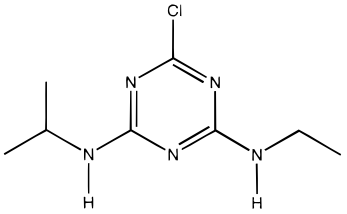

FIGURE 2. Structure of atrazine [2-chloro-6-(ethylamino)-4-isopropylamino-1,3,5-triazine, CIET].

within the complex leading to a charge-transfer state (designated by an asterisk); (ii) lysis of the complex in its charge-transfer state, yielding Fe(II) and $C_2O_4^{\bullet-}$ (*20*); (iii) reaction of the $C_2O_4^{\bullet-}$ radical with molecular oxygen to give 2 CO_2 and $O_2^{\bullet-}$, where $O_2^{\bullet-}$ is in equilibrium with $HO_2^{\bullet}$ [pK_a = 4.8 (*21*)]. The end product of $HO_2^{\bullet}/O_2^{\bullet-}$ dismutation is H_2O_2, by the following reactions (reactions II in Figure 1):

$$2\ HO_2^{\bullet}/O_2^{\bullet-} \xrightarrow{H^+} H_2O_2 + O_2 \qquad (1)$$

$$Fe(II) + HO_2^{\bullet}/O_2^{\bullet-} \xrightarrow{H^+} Fe(III) + H_2O_2 \qquad (2)$$

Hydrogen peroxide formed from $HO_2^{\bullet}/O_2^{\bullet-}$ is another significant oxidant of Fe(II) by the Fenton reaction, yielding $HO^{\bullet}$ (reaction III in Figure 1):

$$Fe(II) + H_2O_2 \rightarrow Fe(III) + HO^{\bullet} + OH^- \qquad (3)$$

The rate constants of Fe(II) oxidation by $HO_2^{\bullet}/O_2^{\bullet-}$ and by H_2O_2 depend critically on the Fe(II) speciation.

Figure 1 shows solely the most relevant reactions that lead ultimately to formation of $HO^{\bullet}$. In these photo-Fenton systems, a number of additional intermediate and side reactions are involved (see Table 1).

Experimental Section

Materials. All reagents were reagent grade. pH measurements were carried out with a combined glass electrode (Methrom) standardized with pH buffer solutions (Merck). Atrazine (CIET) was used as purchased (for the structure of atrazine, see Figure 2). All solutions were prepared in Nanopure water (Q-H_2O grade Barnstead).

Measurement of Hydrogen Peroxide and Iron(II). Hydrogen peroxide was analyzed using the DPD method developed by Bader et al. (*22*), modified to minimize interference by Fe(II) and Fe(III). Bipyridine was added to complex Fe(II); EDTA was added to complex Fe(III). The modified procedure consisted of the following steps: 0.4 mL of phosphate buffer solution (pH 6, 0.5 M phosphate) and 0.1 mL of bipyridine solution (0.01 M) were premixed in a 1 cm quartz cell; 2 mL of the sample, 0.02 mL of EDTA solution (0.01 M NaEDTA), and 0.03 mL of DPD (*N*,*N*-diethyl-*p*-phenylenediamine) reagent (1% in 0.1 M H_2SO_4) were then added, followed by 0.03 mL of POD (horseradish peroxidase) reagent (about 0.8 g/mL). The absorbance at 551 nm was measured.

Fe(II) was measured colorimetrically using the ferrozine method, according to a modified method from Stookey and Lawrence (*23*): 2 mL of the sample was added to 120 μL of H_2SO_4 (3.6 M) in a 1 cm quartz cell and mixed, followed by the addition of 120 μL of ferrozine solution (0.02 M) and 200 μL of ammonium acetate buffer (pH 4.5). The absorbance was measured at the maximal absorption of the iron(II)−ferrozine complex (λ_{max} = 562 nm). At the Fe(II) and oxlalate concentrations used in the experiments, oxalate was not found to interfere with the Fe(II) measurements.

HPLC Analysis of Atrazine. An HPLC system (Hewlett-Packard 1090 Series II/L liquid chromatograph) equipped with a data acquisition system, a diode array detector, and an auto sampler was used for atrazine analysis. For atrazine measurement, an ODS 30 column (Ultracarb 5, 150 × 4.6 mm; Phenomenex, Torrance, CA) and isocratic elution at a flow rate of 0.8 mL min^{-1} were used. As eluent, 50% buffer (0.001 M KH_2PO_4, pH 7.0) and 50% acetonitrile were used. To prevent reactions after sampling and for better HPLC analysis, 0.8 mL of the samples was added to 0.2 mL of methanol in amber HPLC glass vials.

HPLC Analysis of Atrazine Degradation Products. Separation of atrazine and its metabolites was performed using a LiChrosphere 100 RP-18 column (5 μm) from Merck, 250 × 4 mm, and gradient elution. Initial conditions were 95% KH_2PO_4 buffer and 5% acetonitrile isocratic elution for 4 min, followed by a linear gradient to 40% acetonitrile within 18 min, another linear gradient to 60% acetonitrile, reached within 10 min, and a postrun time of 3 min. This separation method allowed the simultaneous measurement of CIET (atrazine), CEAT (deisopropylatrazine), CIAT (deethylatrazine), CAAT (dealkylated atrazine), CDET (simazine amide), CDIT (atrazine amide), OIET (hydroxyatrazine), OEAT (deisopropylhydroxyatrazine), and OIAT (deethylhydroxyatrazine). Absorbance was measured continuously in the range 190−350 nm. Triazine peaks were normally quantified at 220 nm. Besides the retention time, UV peak spectra were used for identification. To prevent reactions after sampling and for better HPLC analysis, 1.0 mL of sample was added to 0.1 mL of methanol. Amber glass vials were used.

Kinetic Experiments. All photochemical and dark control experiments were carried out in a 350 mL Pyrex reactor (cutting off light of wavelengths below 290 nm), equipped with a water jacket at constant temperature (25 ± 1 °C). The solutions were stirred before and throughout the experiments. In the photochemical experiments, the solutions were irradiated with a XENON-short arc lamp (XBO, Osram, maximum output 1000 W) with PTI (Photon Technology International) 02-A5000 arc lamp housing and PTI LPS 1000 power supply. The xenon lamp in combination with Pyrex lenses for UV cutoff at 290 nm was used for sunlight simulation. Irradiation of solutions was performed at 200 W lamp output, corresponding to approximately 500 W m^{-2} which is about half of sunlight intensity at mid-latitude summer noon, as estimated by ferrioxalate actinometry according to refs *6* and *24*. The test volume was 200 mL in all photochemical experiments, corresponding to an optical depth of 3.8 cm. Degradation of atrazine by photochemically generated OH radicals was investigated in $NaClO_4$ as inert electrolyte (I = 0.004 M) at several pH values (3 ≤ pH ≤ 8) in systems containing initially 0.1 mg/L (=0.47 μM) atrazine, 6 μM iron(III) (added as acidic $FeCl_3$ solution), and oxalate (as $K_2C_2O_4$) at initial concentrations of 18 or 180 μM. The pH was adjusted by addition of $HClO_4$ or NaOH and kept constant by automatic titration of $HClO_4$ during the experiments if necessary. In all the experiments, $K_2C_2O_4$ and $NaClO_4$ were added prior to the addition of iron. NaOH for pH adjustment was also added before $FeCl_3$ to prevent precipitation of Fe(III). Atrazine was added after an equilibration time of at least 45 min, followed by another 10 min of equilibration before starting irradiation. The solutions were bubbled with a 20% O_2/80% N_2 mixture (synthetic air) half an hour before and during the experiments in order to keep the oxygen concentration constant.

Software Used for Kinetic Modeling. Concentration vs time curves for diverse system compounds were calculated at pH 3 and for various oxalate concentrations. ACUCHEM, a numerical integration program, was used to compute the time-dependent concentrations of all reactants (*25*). A Matlab program (*26*) and two auxiliary Pascal programs inserted initial concentrations and plotted the calculation results.

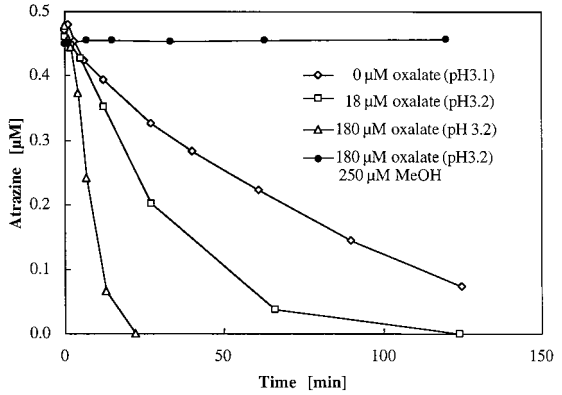

FIGURE 3. Effect of different initial oxalate concentrations (0, 18, and 180 μM) and of excess methanol on atrazine degradation in photo-Fenton systems containing 6 μM total iron and 0.47 μM atrazine (initial concentration) at pH $\approx$ 3.

Results and Discussion

Experimental Evidence for Atrazine Degradation by HO•. Experiments with the HO• scavenger methanol as well as the detected products provide evidence that the only degradation pathway of atrazine was attack by HO• in the investigated photo-Fenton systems. In irradiated, oxygen-saturated solutions containing initially 6 μM Fe(III), 180 μM oxalate, 0.47 μM atrazine, and 250 μM methanol, no degradation of atrazine was found, neither at pH 3.2 nor at pH 4.7. In contrast, atrazine degradation occurred rapidly in the absence of methanol under otherwise the same conditions (Figure 3). The formation and degradation of several atrazine metabolites at pH 3.4, 60 μM total iron, initial [oxalate] = 1.8 mM, and [atrazine] = 5 μM was followed (data not shown). The major products were CEAT (deisopropylatrazine), CIAT (deethylatrazine), and CDIT (6-acetamido-2-chloro-4-isopropylamino-1,3,5-triazine). CDET [4-acetamido-2-chloro-6-(ethylamino)-1,3,5-triazine] was a minor product. CAAT (dealkylated atrazine) was formed as a secondary metabolite when CEAT and CIAT concentrations decreased. No detectable amounts of the hydroxylated triazines OIET (hydroxyatrazine), OIAT (deethylhydroxyatrazine), and OEAT (deisopropylhydroxyatrazine) were found. These findings are consistent with the work of Torrents and co-workers (*17*) and Hapeman et al. (*27*, *28*), who studied atrazine degradation by HO• formed by NO_3^- photolysis and ozonation, respectively. In addition, control experiments showed no atrazine degradation neither by direct photolysis nor in dark systems during several hours (data not shown).

Effect of Oxalate Concentration and pH on Atrazine Degradation in Photo-Fenton Systems. Figure 3 shows the atrazine degradation by HO• at initial oxalate concentrations of 0, 18, and 180 μM at pH 3.1−3.2. The degradation rate of atrazine (initially 0.47 μM) in these irradiated systems, containing 6 μM total iron, increased with oxalate concentration.

The oxalate dependence of the kinetics of atrazine degradation can be explained by the speciation of Fe(III) (Figure 4a,b). In systems containing 18 and 180 μM oxalate at pH 3, Fe(III) is mainly present as $Fe(C_2O_4)^+$ and $Fe(C_2O_4)_2^-$, and as $Fe(C_2O_4)_2^-$ and $Fe(C_2O_4)_3^{3-}$, respectively. In the absence of oxalate, a fraction of more than 60% of Fe(III) is present as $Fe(OH)^{2+}$ at this pH (calculation data not shown). Since $Fe(C_2O_4)_2^-$ and $Fe(C_2O_4)_3^{3-}$ are much more efficently photolyzed than $Fe(C_2O_4)^+$ and $Fe(OH)^{2+}$ (see kinetic modeling), the formation of Fe(II) and H_2O_2 is faster at high oxalate concentration.

Atrazine degradation was also strongly dependent on pH, both in the presence of oxalate (18 or 180 μM) and in its absence (Figure 5a−c). At an initial oxalate concentration of

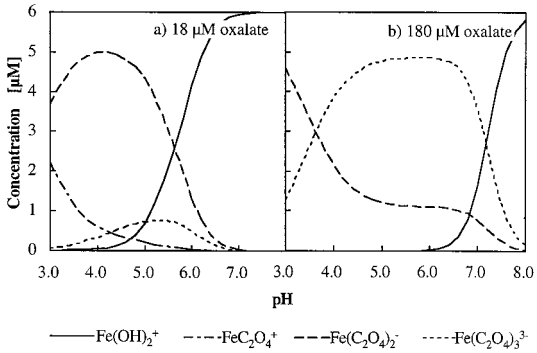

FIGURE 4. Iron(III) speciation as a function of pH in calculated systems containing 6 μM Fe(III) and 18 μM oxalate (a) or 180 μM oxalate (b). Data were calculated by the speciation program MICROQL (*33*). With regard to slow formation of solid phases on the time scale of the experiments, solid iron phases [e.g., $Fe(OH)_3$] were not included in the calculation. All equilibrium constants were taken from ref *34* and corrected for 4 mM ionic strength using the Davies equation.

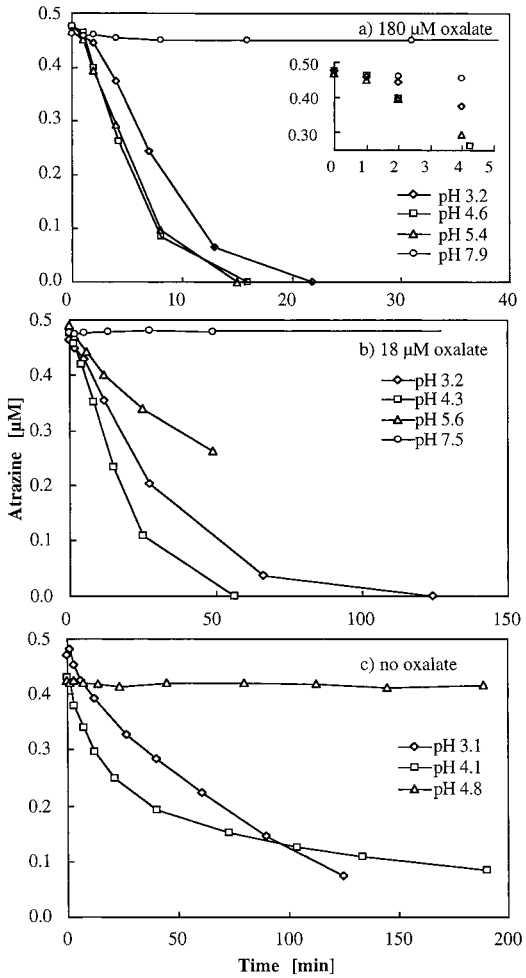

FIGURE 5. pH dependence of atrazine degradation in photo-Fenton systems containing 6 μM total iron, and 180 μM (a), 18 μM (b), and no oxalate (c). The inset shows the induction period during the first 5 min after irradiation.

18 μM, a loss of >99.5% of atrazine was observed within 1 h at pH 4.3 and within 2 h at pH 3.2. At pH 5.6, only 60% of the initial amount was transformed within 6 h, and no transformation occurred at pH higher than 7. These experimental observations can be explained by the following pH effects: (i) The concentrations of the most efficiently photolyzed species, $Fe(C_2O_4)_2^-$ and $Fe(C_2O_4)_3^{3-}$, are highest

around pH 4 (Figure 4a). In the irradiated pH 7.5 system, atrazine was found to be stable because of the absence of any ferric iron species that could be efficiently photolyzed. (ii) The pH also controls the Fe(II) speciation, affecting the rate of the Fenton reaction: Fe^{2+}, which is the predominant Fe(II) species at low pH and low oxalate concentrations, is oxidized by H_2O_2 at a rate constant of $53-76\ M^{-1}\ s^{-1}$ (literature values from refs *7*, *29*, *30*). With increasing pH and oxalate concentration, $[Fe^{II}(C_2O_4)]$ increases, according to a speciation calculation (data not shown). $Fe^{II}(C_2O_4)$ is oxidized by H_2O_2 at a rate constant of $k = 3 \times 10^4\ M^{-1}\ s^{-1}$ (*7*). Therefore, the Fenton reaction, resulting in $HO^\bullet$ generation, is faster at higher pH. $Fe^{II}(OH)^+$ would be oxidized by H_2O_2 at a rate of $>1 \times 10^6\ M^{-1}\ s^{-1}$ (*7*) but was calculated to occur only at negligible concentrations. (iii) The solubility of iron(III) strongly decreases with increasing pH. [Note that at pH values even lower than 7.5 dissolved Fe(III) may not be in equilibrium with the solid phase after oxalate consumption, due to slow precipitation kinetics, resulting in a decrease of the atrazine transformation rate.]

The iron speciation in the systems initially containing 180 μM oxalate was calculated to be approximately the same within the pH range 4.4−6.6, essentially $Fe(C_2O_4)_3^{3-}$ (Figure 4b). This concurs with the observed atrazine transformation rate at pH 4.6 and 5.4, which are similar (Figure 5a). The inset in Figure 5a shows a lag period, where atrazine was not degraded during the first 5 min after the start of irradiation, independent of pH. This is because H_2O_2 and Fe(II) first have to be formed before the Fenton reaction can start to produce $HO^\bullet$ that degrade atrazine.

In the systems without oxalate, Fe(II) and $HO^\bullet$ radicals were generated by photolysis of Fe-hydroxo species. $Fe(OH)^{2+}$ as well as the binuclear $Fe_2(OH)_2^{4+}$ are photolyzed (*11*). Since the solutions were not in equilibrium with the solid phase, the iron speciation can hardly be calculated. In these systems, the degradation kinetics at pH 3 and 4 (Figure 5c) are difficult to interpret quantitatively. The distinct decrease of the atrazine degradation rate with time at pH 4.1 can be explained by slow precipitation of Fe(III).

Atrazine degradation in these systems cannot be described by a simple pseudo-first-order rate law ($r = k_{CIET,\ HO^\bullet}[HO^\bullet]_{ss}[CIET]$), since the steady-state concentration of $HO^\bullet$ changes, due to changing conditions during the experiments. A decrease in the $HO^\bullet$ production rate is caused by consumption of oxalate by photolysis of $Fe(C_2O_4)_2^-$ and $Fe(C_2O_4)_3^{3-}$. Furthermore, in the system with 180 μM initial oxalate, $HO^\bullet$ consumption by free oxalate species, $C_2O_4^{2-}$ and $HC_2O_4^-$, may be of the same order of magnitude as that of the atrazine reaction with $HO^\bullet$. At an initial oxalate concentration of 18 μM, the amount of free oxalate species at pH values below 5.5 is small and should not affect the $HO^\bullet$ concentration. Thus, both oxalate concentration and pH and hence iron(III) speciation and the presence of free oxalate determine the $HO^\bullet$ concentration in the photo-Fenton systems by affecting the rate coefficient of photolysis of Fe(III) species as well as the rate of hydroxyl radical consumption. Oxalate concentration and pH also affect $[HO^\bullet]$ through the rate of the Fenton reaction which in turn depends on Fe(II) speciation.

Kinetic Modeling of Fe(II), H_2O_2, and Atrazine Dynamics. To get more information on iron cycling that accompanied atrazine degradation and to identify the most important equilibria and reactions, Fe(II) and hydrogen peroxide were measured and kinetic calculations were carried out, using ACUCHEM (Figures 6a−d and 7). In all systems (18 and 180 μM initial oxalate, each at about pH 3 and 5), maximal Fe(II) concentration was around half of total iron concentration (6 μM). H_2O_2 concentrations were highest at low pH and high oxalate concentration and increased to maximal values

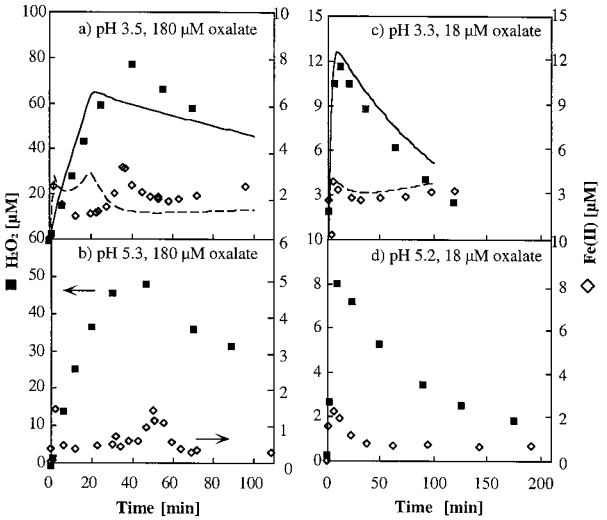

FIGURE 6. Formation and consumption of H_2O_2 (■, left scale) and of Fe(II) (◇, right scale) in different photo-Fenton systems: (a) pH 3.5, 180 μM oxalate; (b) pH 5.3, 180 μM oxalate; (c) pH 3.3, 18 μM oxalate; and (d) pH 5.2, 18 μM oxalate. All systems contained 6 μM total iron and initially 0.47 μM atrazine. Calculated concentration vs time courses: H_2O_2 (—) and Fe(II) (- - -) at pH 3.2.

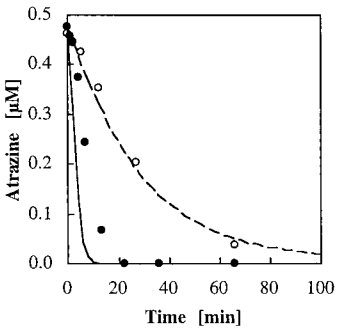

FIGURE 7. Calculated concentration vs time courses and experimental data of atrazine in photo-Fenton systems at pH 3.2 containing 6 μM total iron, initially 0.47 μM atrazine, and various initial oxalate concentrations. System with initial [oxalate] = 18 μM: (- - -) calculated, (○) experimental; system with initial [oxalate] = 180 μM: (—) calculated, (●) experimental.

of 8−12 μM (system containing 18 μM initial oxalate) and 50−80 μM (180 μM initial oxalate). These measurements are consistent with the dependence of atrazine degradation on pH and on the oxalate concentration. The dynamics of Fe(II) and H_2O_2 concentrations are a result of numerous concurrent processes in the systems and can therefore hardly be explained quantitatively without using an appropriate kinetic model.

For kinetic modeling, the set of reactions and equilibria and the corresponding constants listed in Table 1 were used. None of the rate constants are fitted values. For most rate or equilibrium constants, literature values were used. We calculated the photolysis rate coefficients, k_p, of different Fe(III) species in these systems, where k_p is

$$k_p = \sum [k_a(\lambda) \cdot \Phi(\lambda)]\ \Delta\lambda \qquad (4)$$

$k_a(\lambda)$ is the specific rate of light absorption at wavelength λ, and $\Phi(\lambda)$ is the quantum yield at λ. We calculated k_a, the total specific rate of light absorption, for the experimental systems (initial conditions) with excess oxalate and without oxalate at pH 3, by summation of $k_a(\lambda)$ in the wavelength range where the lamp spectrum and the absorption spectra of

TABLE 1. Reactions and Rate Constants, *k*, or Equilibrium Constants, *K*, for Kinetic Modeling

reaction	*k* or *K*	reference
photolysis of Fe(III) species[a]		
1 $Fe^{III}(C_2O_4)_2^- \xrightarrow{h\nu} Fe^{II}(C_2O_4) + C_2O_4^{-\bullet}$	$k = 0.04\ s^{-1}$	*b*
2 $Fe^{III}(C_2O_4)_3^{3-} \xrightarrow{h\nu} Fe^{II}(C_2O_4)_2^{2-} + C_2O_4^{-\bullet}$	$k = 0.04\ s^{-1}$	*b*
3 $Fe^{III}(OH)^{2+} \xrightarrow{h\nu} Fe^{2+} + HO^\bullet$	$k = 0.0012\ s^{-1}$	*b*
4 $C_2O_4^{-\bullet} \rightarrow CO_2 + CO_2^{-\bullet}$	$k = 2 \times 10^6\ s^{-1}$	(*35*)
5 $CO_2^{-\bullet} + O_2 \rightarrow CO_2 + O_2^{-\bullet}$	$k = 2.4 \times 10^9\ M^{-1}\ s^{-1}$	(*7*)
Fe reductions and oxidations[d]		
6 $Fe^{3+} + O_2^{-\bullet} \rightarrow O_2 + Fe^{2+}$	$k = 1.5 \times 10^8\ M^{-1}\ s^{-1}$	(*29*)
7 $Fe^{3+} + HO_2^\bullet \xrightarrow{-H^+} O_2 + Fe^{2+}$	$k = 1 \times 10^6\ M^{-1}\ s^{-1}$	(*36*)
8 $Fe^{III}(C_2O_4)_n^{3-2n} + O_2^{-\bullet} \rightarrow O_2 + Fe^{II}(C_2O_4)_n^{2-2n}$	$k = 1 \times 10^5\ M^{-1}\ s^{-1}$	(*7*)[c]
9 $Fe^{III} + (C_2O_4)_n^{3-2n} + HO_2^\bullet \xrightarrow{-H^+} O_2 + Fe^{II}(C_2O_4)_n^{2-2n}$	$k = 1.2 \times 10^4\ M^{-1}\ s^{-1}$	(*7*)[c]
10 $Fe^{2+} + O_2^{-\bullet} \xrightarrow{2H^+} Fe^{3+} + H_2O_2$	$k = 1 \times 10^7\ M^{-1}\ s^{-1}$	(*7*, *29*)
11 $Fe^{2+} + HO_2^\bullet \xrightarrow{H^+} Fe^{3+} + H_2O_2$	$k = 1.2 \times 10^5\ M^{-1}\ s^{-1}$	(*7*, *29*)
Fenton reactions[e]		
12 $Fe^{2+} + H_2O_2 \rightarrow Fe^{3+} + HO^\bullet + OH^-$	$k = 53\ M^{-1}\ s^{-1}$	(*30*)
13 $Fe^{II}(C_2O_4) + H_2O_2 \rightarrow Fe^{III}(C_2O_4)^+ + HO^\bullet + OH^-$	$k = 3.1 \times 10^4\ M^{-1}\ s^{-1}$	(*7*)
$HO^\bullet$ reactions[f]		
14 $C_2O_4^{2-} + HO^\bullet \rightarrow CO_2 + CO_2^{-\bullet} + OH^-$	$k = 7.7 \times 10^6\ M^{-1}\ s^{-1}$	(*7*)
15 $HC_2O_4^- + HO^\bullet \rightarrow CO_2 + CO_2^{-\bullet} + H_2O$	$k = 4.7 \times 10^7\ M^{-1}\ s^{-1}$	(*7*)
16 atrazine + $HO^\bullet \rightarrow$ products	$k = 3 \times 10^9\ M^{-1}\ s^{-1}$	(*3*)
17 P + $HO^\bullet \rightarrow$ P	$k = 3 \times 10^9\ M^{-1}\ s^{-1}$	*b*
18 $Fe^{2+} + HO^\bullet \rightarrow Fe^{III}(OH)^{2+}$	$k = 4.3 \times 10^8\ M^{-1}\ s^{-1}$	(*37*)
19 $H_2O_2 + HO^\bullet \rightarrow HO_2^\bullet + H_2O$	$k = 3 \times 10^7\ M^{-1}\ s^{-1}$	(*38*)[g]
$HO_2^\bullet/O_2^{-\bullet}$ reactions and equilibria		
20 $HO_2^\bullet + HO_2^\bullet \rightarrow H_2O_2 + O_2$	$k = 8.3 \times 10^5\ M^{-1}\ s^{-1}$	(*29*)
21 $HO_2^\bullet + O_2^{-\bullet} \xrightarrow{H^+} H_2O_2 + O_2$	$k = 9.7 \times 10^7\ M^{-1}\ s^{-1}$	(*29*)
22 $HO_2^\bullet \rightleftarrows O_2^{-\bullet} + H^+$	$K = 1.58 \times 10^{-5}$ M	(*6*)
iron and oxalate equilibria[e,h]		
23 $Fe^{2+} + C_2O_4^{2-} \rightleftarrows Fe^{II}(C_2O_4)$	$K = 4.17 \times 10^3\ M^{-1}$	(*34*)
24 $Fe^{II}(C_2O_4) + C_2O_4^{2-} \rightleftarrows Fe^{II}(C_2O_4)_2^{2-}$	$K = 1.26 \times 10^2\ M^{-1}$	(*34*)
25 $Fe^{3+} + C_2O_4^{2-} \rightleftarrows Fe^{III}(C_2O_4)^+$	$K = 5.89 \times 10^8\ M^{-1}$	(*34*)
26 $Fe^{III}(C_2O_4)^+ + C_2O_4^{2-} \rightleftarrows Fe^{III}(C_2O_4)_2^-$	$K = 3.31 \times 10^6\ M^{-1}$	(*34*)
27 $Fe^{III}(C_2O_4)_2^- + C_2O_4^{2-} \rightleftarrows Fe^{III}(C_2O_4)_3^{3-}$	$K = 2.75 \times 10^4\ M^{-1}$	(*34*)
28 $HC_2O_4^- \rightleftarrows C_2O_4^{2-} + H^+$	$K = 6.61 \times 10^{-5}$ M	(*34*)
29 $Fe^{3+} + H_2O \rightleftarrows Fe^{III}(OH)^{2+} + H^+$	$K = 4.57 \times 10^{-3}$ M	(*34*)
30 $Fe^{III}(OH)^{2+} + H_2O \rightleftarrows Fe^{III}(OH)_2^+ + H^+$	$K = 2.51 \times 10^{-4}$ M	(*34*)

[a] Photolysis of $Fe^{III}(C_2O_4)^+$ was not considered due to its inefficiency (*39*). [b] Estimated as described in the text. P in reaction 17 stands for organic compounds present in the water used (see text). [c] Values given by reference *7*: $k \leq 1 \times 10^6\ M^{-1}\ s^{-1}$ and $k \leq 1.2 \times 10^5\ M^{-1}\ s^{-1}$ for reactions 8 and 9, respectively. [d] Oxidation of iron(II) by O_2 is negligible at low pH (*6*). [e] $Fe^{II}(OH)^+$ occurs only at very small concentration and was neglected. [f] The reaction of Cl^- (added as $Fe^{III}Cl_3$) and of atrazine metabolites with $HO^\bullet$ did not affect the calculated results. [g] Reaction rate constant given by reference *38*: $1.2 \leq k \leq 4.5 \times 10^7\ M^{-1}s^{-1}$. [h] All equilibrium constants were corrected for ionic strength $I = 4$ mM with the Davies equation. $Fe^{III}(OH)_3$(s) was not important until oxalate was consumed. Therefore and because equilibrium between solution Fe(III) and solid phases is slowly established, $Fe^{III}(OH)_3$(s) was not considered in the model. Because ACUCHEM is dealing with forward reactions only, equilibria were split into forward and back reactions. The rate constants of the forward and back reactions, k_{for} and k_{back}, respectively, were chosen such that $K = k_{for}/k_{back}$, whereas one of the two was assumed to be high ($>10^9$).

$Fe(C_2O_4)_n^{(3-2n)}$ or $Fe(OH)^{2+}$ overlap (300 nm $\leq \lambda \leq$ 500 nm):

$$k_a = \sum k_a(\lambda)\cdot\Delta\lambda = \sum \frac{I_0(\lambda)\cdot(1 - 10^{-\epsilon(\lambda)lc})}{l\cdot c}\cdot\Delta\lambda \qquad (5)$$

$I_0(\lambda)$ = spectral photon flux of the light source in the interval $\lambda-\Delta\lambda/2$ to $\lambda+\Delta\lambda/2$ [photons $cm^{-2}\ s^{-1}\ nm^{-1}$] (spectrum as specified by producer), l = light path length, $\epsilon(\lambda)$ = molar decadic extinction coefficient, and c = concentration of absorbing species. Since the light absorption by the absorbing species is small, eq 5 can be simplified:

$$k_a \approx \sum [I_0(\lambda)2.3\epsilon(\lambda)]\Delta\lambda \qquad (6)$$

$k_{a(Fe(C_2O_4)_n^{(3-2n)})}$ was calculated to be 0.079 s^{-1} and $k_{a(Fe(OH)^{2+})} = 0.018\ s^{-1}$. We assumed constant quantum yields Φ within the relevant wavelength range (300−500 nm). This simplification is reasonable since within this wavelength range the quantum yield of Fe(II) production changes only slightly [$0.9 \leq \Phi_{Fe(II)\ production} \leq 1.3$ between 300 and 500 nm under nitrogen (*31*)] and $Fe(OH)^{2+}$ is less relevant than $Fe(C_2O_4)_n^{(3-2n)}$ in our systems. For the calculation of k_p, we used the quantum yield $\Phi(\lambda)$ at the wavelength λ where $k_a(\lambda)$ was maximal. The value of $\Phi(350\ nm)_{Fe(C_2O_4)_n^{(3-2n)}-photolysis} = 0.56$ was obtained by dividing the value determined by ref *31* under nitrogen by 2, because the presence of oxygen reduces the quantum yield of Fe(II) formation by half. $\Phi(340\ nm)_{Fe(OH)^{2+}-photolysis} = 0.07$ was estimated by interpolating two values given by ref *11* at 313 nm ($\Phi = 0.14$) and at 360 nm ($\Phi = 0.017$). Hence, photolysis rate coefficients were calculated to be $k_{p(Fe(C_2O_4)_n^{3-2n})} \approx 0.044\ s^{-1}$ and $k_{p(Fe(OH)^{2+})} \approx 0.0012\ s^{-1}$.

Not only k_p but also the use of some rate constants taken from the literature is subject to uncertainty, since they were determined under different experimental conditions. Nevertheless, the calculated concentration vs time courses of Fe(II), of H_2O_2, and of atrazine agree reasonably well with the experimental data points at pH 3 (Figure 6a,b), suggesting that the model considers the most important reactions and equilibria of the test systems at low pH. At inital [oxalate] = 180 μM, the maxima in the Fe(II) and H_2O_2 concentrations

were calculated to occur at earlier times than experimentally observed (after 40 min), but in agreement with experimental values, the model also predicts that maximal Fe(II) and H_2O_2 concentrations occur concomitantly. The calculated concentration vs time course of Fe(II) was markedly influenced by the value of k_p. Reducing k_p in the model by a factor of 2 led to a better agreement of Fe(II) with the experimental data, but underestimated the atrazine degradation rate at [oxalate] = 18 μM. At pH 5, calculated results were not in good agreement with the experimental data. At this pH, also precipitation of Fe(III) would have to be taken into account in the modeling which is hardly feasible because equilibria are slowly established in these systems.

The Nanopure water used for the test solutions contained up to 0.5 mg L^{-1} of total organic carbon (TOC) that could have acted as OH radical scavenger. Without these impurities, the calculated [HO$^\bullet$] and hence the atrazine degradation rate would have been higher by a factor of 10. Therefore, an unknown HO$^\bullet$ scavenger (P) at a concentration of [P] = 5 μM was included in the model. We assumed a reaction rate constant of HO$^\bullet$ with P of $k = 3 \times 10^9$ M^{-1} s^{-1}.

Qualitatively, the courses of Fe(II) and H_2O_2 at 180 μM intial oxalate can be interpreted as a result of subsequent and concurrent reactions: Fe(II) and $O_2^{\bullet-}/HO_2^\bullet$ production by photolysis of Fe(III)−oxalate complexes starts immediately with irradiation. As a second step, reoxidation of Fe(II) by $O_2^{\bullet-}/HO_2^\bullet$ produced H_2O_2. In the 180 μM oxalate system, [Fe(II)] therefore increased faster at the beginning than did [H_2O_2]. Since H_2O_2 oxidized Fe(II) to produce HO$^\bullet$, ferrous iron decreased after a first maximum after about 2 min of irradiation, while hydrogen peroxide was further increasing. The reoxidation of Fe(II) increased the photolysis rate because of re-formation of ferric−oxalate complexes, yielding a second maximum in the Fe(II) concentration. The following decrease in the H_2O_2 concentration can be explained by consumption of oxalate, causing slower photolysis of Fe(III) complexes (see above).

The calculated OH radical concentration was in the range of about (0.2−3.5) $\times 10^{-12}$ M. A distinct peak was obtained after about 10 min of irradiation in the system with inital 180 μM oxalate, whereas at inital 18 μM oxalate, calculated [HO$^\bullet$] was about 0.1 $\times 10^{-12}$ M and varied only slightly within the considered time range. Note that the calculated HO$^\bullet$ concentrations are high compared to those in natural waters [e.g., in the epilimnion of Lake Greifensee, $[HO^\bullet]_{ss} \approx 10^{-16}$ M *(32)*].

Environmental Significance. This study elucidates the effects of organic Fe(III) complexing agents and of pH on the kinetics of atrazine degradation by HO$^\bullet$ produced in photo-Fenton systems. Both factors strongly affect the rate of HO$^\bullet$ formation by controlling the Fe(III) and Fe(II) speciation and thus the rates of photolysis and of the Fenton reaction, respectively. Hence, iron speciation is a key parameter in photo-Fenton systems. The investigations on the effect of pH show that photo-Fenton systems are very inefficient at neutral or higher pH, even in the presence of organic complexing compounds, mainly because of the effect of pH on Fe(III) speciation. In environmental compartments with low pH, i.e., atmospheric waters or iron-rich acidic surface waters, the efficiency of pollutant degradation by these processes critically depends on the presence and concentration of organic complexing agents. Organic substances such as oxalate or humic and fulvic acids play a multiple role in these systems since they affect [HO$^\bullet$] in opposite ways: (i) Organically complexed Fe(III) is more efficiently photolyzed than inorganic Fe(III). (ii) Organically complexed Fe(II) is faster oxidized. (iii) Organic complexing agents also act as HO$^\bullet$ scavengers. The effect of different, naturally occurring organic compounds should be subject to further studies. Due to the low solubility of Fe(III) over a wide pH range, a large fraction of Fe(III) is present as amorphous or crystalline Fe(III)-oxides or -hydroxides in most environmental systems. A pertinent question which remains to be answered is the significance of pollutant degradation by HO$^\bullet$ that are produced on surfaces of iron-containing solid phases.

Acknowledgments

We thank René P. Schwarzenbach and Silvio Canonica for critical discussion and Stephan J. Hug for providing the tools for kinetic modeling and for his help with defining the model as well as for critical discussion.

Literature Cited

(1) Zepp, R. G.; Hoigné, J.; Bader, H. *Environ. Sci. Technol.* **1987**, *21*, 443−450.
(2) Buxton, G. V.; Greenstock, C. L.; Helman, W. P.; Ross, A. B. *J. Phys. Chem. Ref. Data* **1988**, *17*, 513−886.
(3) Haag, W. R.; Yao, C. C. D. *Environ. Sci. Technol.* **1992**, *26*, 1005−1013.
(4) Zepp, R. G.; Faust, B. C.; Hoigné, J. *Environ. Sci. Technol.* **1992**, *26*, 313−319.
(5) Voelker, B. M.; Sulzberger, B. *Environ. Sci. Technol.* **1996**, *30*, 1106−1114.
(6) Voelker, B. M.; Morel, F. M. M.; Sulzberger, B. *Environ. Sci. Technol.* **1997**, *31*, 1004−1011.
(7) Sedlak, D. L.; Hoigné, J. *Atmos. Environ.* **1993**, *27A*, 2173−2185.
(8) Haag, W. R.; Hoigné, J. *Chemosphere* **1985**, *14*, 1659−1671.
(9) Mopper, K.; Zhou, X. *Science* **1990**, *250*, 661−664.
(10) Sigleo, A. C.; Cunningham, K. M.; Goldberg, M. C.; Kimball, B. A. In *U. S. Geological Survey Toxic Substances Hydrology Program*, Vol. Report 88-4220, Denver, CO, Phoenix, AZ; U.S. Geological Survey Water-Resources Investigations, 1988; pp 125−129.
(11) Faust, B. C.; Hoigné, J. *Atmos. Environ.* **1990**, *24A*, 79−89.
(12) Sposito, G. *The Surface Chemistry of Soils*; Oxford University Press: Oxford, U.K., 1989.
(13) Erikson, L. E.; Lee, K. H. *Crit. Rev. Environ. Control* **1989**, *19*, 1−14.
(14) Muir, D. C. G.; Baker, B. E. *Weed Res.* **1978**, *18*, 111−120.
(15) Ulrich, M. M.; Müller, S. R.; Singer, H. P.; Imboden, D. M.; Schwarzenbach, R. P. *Environ. Sci. Technol.* **1994**, *28*, 1674−1684.
(16) Kolpin, D. W.; Kalkhoff, S. J. *Environ. Sci. Technol.* **1993**, *27*, 134−139.
(17) Torrents, A.; Anderson, B. G.; Bilboulian, S.; Johnson, W. E.; Hapeman, C. *Environ. Sci. Technol.* **1997**, *31*, 1476−1482.
(18) Arnold, S. M.; Hickey, W. J.; Harris, R. F. *Environ. Sci. Technol.* **1995**, *29*, 2083−2089.
(19) Pelizzetti, E.; Minero, C.; Carlin, V.; Vincenti, M.; Pramauro, M.; Dolci, M. *Chemosphere* **1992**, *24*, 891−910.
(20) Balzani, V.; Carassiti, V. *Photochemistry of coordination compounds*; Academic Press: London, 1970.
(21) Bielski, B. H. J.; Cabelli, D. E.; Arudi, R. L.; Ross, A. B. *J. Phys. Chem. Ref. Data* **1995**, *14*, 1041−1051.
(22) Bader, H.; Sturzenegger, V.; Hoigné, J. *Water Res.* **1988**, *22*, 1109−1115.
(23) Stookey, L. L. *Anal. Chem.* **1970**, *42*, 779−781.
(24) *Handbook of Photochemistry*, Second Ed., revised and expanded ed.; Murov, S. L., Carmichael, I., Hug, G. L., Eds.; Marcel Dekker: New York, Basel, and Hong Kong, 1993.
(25) Braun, W.; Herron, J. T.; Kahaner, D. In National Bureau of Standards: Gaithersburg, MD, 1986.
(26) Herskovitz, S. In The Math Works, Inc.: Natick, MA, 1989.
(27) Hapeman, C. J.; Karns, J. S.; Shelton, D. R. *J. Agric. Food Chem.* **1995**, *43*, 1383−1391.
(28) Hapeman-Somich, C. J.; Gui-Ming, Z.; Lubsy, W. R.; Muldoon, M. T.; Waters, R. *J. Agric. Food Chem.* **1992**, *40*, 2294−2298.
(29) Zuo, Y.; Hoigné, J. *Environ. Sci. Technol.* **1992**, *26*, 1014−1022.
(30) Pignatello, J. J.; Baehr, K. *J. Environ. Qual.* **1994**, *23*, 365−370.
(31) Hatchard; Parker *Proc. R. Soc. London* **1956**, *A 235*, 518−536.
(32) Schwarzenbach, R. P.; Gschwend, P. M.; Imboden, D. M. *Environmental Organic Chemistry*; John Wiley and Sons: New York, 1992; p 681.

(33) Westall, J. C. "MICROQL-I. A chemical Equilibrium Program in Basic. Version 2 for PC's," Department of Chemistry, Oregon Sate University, Corvallis, OR, 1986.
(34) Smith, R. M.; Martell, A. E. *Critical Stability Constants*; Plenum Press: New York, 1976; Vol. 2 and 3 Inorganic Complexes/Other Organic Ligands.
(35) Mulazzani, Q. G.; D'Angelantonio, M.; Venturi, M.; Hoffmann, M. Z.; Rodgers, A. J. *J. Phys. Chem.* **1986**, *90*, 5347−5352.
(36) Sehested, K.; Bjergbakke, E.; Rasmussen, O. L.; Fricke, H. *J. Chem. Phys.* **1969**, *51*, 3159−3166.
(37) Christensen, H.; Sehested, K. *Radiat. Phys. Chem.* **1981**, *18*, 723−731.
(38) Walling, C. *Acc. Chem. Res.* **1975**, *8*, 125−131.
(39) Vincze, L.; Papp, S. *J. Photochem.* **1987**, *36*, 289−296.

Received for review August 25, 1998. Revised manuscript received March 31, 1999. Accepted April 12, 1999.

ES9808705